

A few filters are enough: Convolutional Neural Network for P300 Detection

Montserrat Alvarado-González^{a,1}, Gibran Fuentes-Pineda^{b,1}, Jorge Cervantes-Ojeda^a

^a*Department of Applied Mathematics and Systems, Universidad Autónoma Metropolitana, 05348, Mexico City, Mexico*

^b*Department of Computer Science, Instituto de Investigaciones en Matemáticas Aplicadas y en Sistemas, Universidad Nacional Autónoma de México, 04510, Mexico City, Mexico*

Abstract

Over the past decade, convolutional neural networks (CNNs) have become the driving force of an ever-increasing set of applications, achieving state-of-the-art performance. Most of the modern CNN architectures are composed of many convolutional and fully connected layers and typically require thousands or millions of parameters to learn. CNNs have also been effective in the detection of Event-Related Potentials from electroencephalogram (EEG) signals, notably the P300 component which is frequently employed in Brain-Computer Interfaces (BCIs). However, for this task, the increase in detection rates compared to approaches based on human-engineered features has not been as impressive as in other areas and might not justify such a large number of parameters. In this paper, we study the performances of existing CNN architectures with diverse complexities for single-trial within-subject and cross-subject P300 detection on four different datasets. We also proposed SepConv1D, a very simple CNN architecture consisting of a single depthwise separable 1D convolutional layer followed by a fully connected Sigmoid classification neuron. We found that with as few as four filters in its convolutional layer and a small overall number of parameters, SepConv1D obtained competitive performances in the four datasets. We believe this may represent an important step towards building simpler, cheaper, faster, and more portable BCIs.

Keywords: Convolutional Neural Network, P300, single-trial, within-subject,

*Corresponding author

Email address: amontserrat@gmail.com (Montserrat Alvarado-González)

¹These authors contributed equally to this work.

1. Introduction

A Brain-Computer Interface (BCI) is a system composed of software and hardware that builds a channel of communication between the subject and the computer, using only the subject's brain signals [1]. The general process followed by a BCI can be divided into: subject's stimulation, acquisition of brain activity, signal preprocessing, feature extraction, classification, and translation of the output's classification into instructions to control an application or a device. One of the brain signals captured with the electroencephalogram (EEG) of interest in the community for controlling BCIs is the Event-Related Potential (ERP). In particular, the late P300 component has a stable temporal relationship with respect to the stimulation event, an interesting characteristic to control BCIs. For instance, it is related to cognitive and attention processes and it is independent of the type of stimulation presented to the subject. The P300 is associated with the oddball paradigm, which consists in presenting a series of frequent stimuli interrupted by infrequent stimuli [2]. Thus, every time the infrequent stimulus is detected by the subject, his brain unconsciously generates a positive peak, approximately 300 ms afterwards.

Given that a BCI based on ERP signals is highly subject-specific, it requires two phases to be used: *i)* an offline training phase to calibrate the system for each subject and *ii)* an online phase to actually let the subject control the BCI. Typically, the subject has to repeat several times the oddball paradigm to increase the ERP's signal-to-noise ratio [3]. Since the stimulation process can become unacceptably slow and tiring for the subject, much of the effort in the BCI development is to stimulate the subject as few times as possible, preferably only once (i.e., by a single-trial), while still achieving an adequate detection of the P300 component. More recently, some works have attempted to eliminate the calibration stage for each subject by using instead the information acquired previously for other subjects [4]. The P300 detection based on the information retrieved during the calibration stage by a single subject is known as within-subject classification, whereas the detection based on the information retrieved

by other subjects is known as cross-subject classification.

In order to detect the P300 under these conditions, a large number of feature extraction, feature selection, and classification methods have been applied by the BCI community. Some of these methods rely on human-engineered features that require significant expertise [5]. The authors of [6] explained that once extracted, the features are selected to: *i*) reduce redundancy, *ii*) choose the ones related to the mental states targeted by the BCI, *iii*) generate fewer parameters to be optimized by the classifier, and *iv*) produce faster predictions for a new sample. Among the most prominent feature selection approaches used for P300 detection are the embedded methods (e.g., Stepwise Linear Discriminant Analysis [7]) and the wrapper methods (e.g., Genetic Algorithms [8]). On the other hand, the approaches more commonly used for P300 classification have been the Linear Discriminant Analysis [9], Support Vector Machines [10], Feed Forward Neural Networks [11, 12], and adaptive classifiers [13, 14].

Recently, some methods merge feature extraction, feature selection, and classification by using matrix classifiers (e.g. [15]) or Deep Learning with Convolutional Neural Networks (CNN) (e.g. [16, 17, 4]). In particular, the latter has gained a lot of interest since it has demonstrated to be very effective in fields such as Computer Vision [18] and Speech Recognition [19], not only to replace human-engineered features but also to increase classification rates. Some characteristics of these methods are their depth, the use of a large number of parameters, and the need of huge amounts of data to train. These characteristics may be a disadvantage for P300 detection, mainly due to the limited training data available [20, 6].

Although CNN architectures have been effective for single-trial within-subject and cross-subject P300 detection from EEG signals, the increase in detection rates compared to approaches based on human-engineered features has not been as impressive as in other areas [21] and might not justify such a large number of parameters. In this paper, we study the performances of the state-of-the-art CNN architectures with diverse complexities for single-trial within-subject and cross-subject P300 detection on four different datasets. We also propose SepConv1D, a very simple CNN architecture consisting of a single depthwise separable 1D convolutional layer followed by a fully connected Sigmoid classification neuron. We compare the state-of-the-art architectures

with SepConv1D and a simple Fully-Connected Neural Network (FCNN) with a single hidden layer with only two neurons, both in terms of detection performance and complexity.

The remainder of this paper is organized as follows. In Section 2, we review the state-of-the-art CNN architectures for P300 detection. In Section 3, we describe in detail SepConv1D and a simple Fully-Connected Neural Network. In Section 4, we present the experimental design and the datasets. Section 5 shows the results of the experimental evaluation and discusses the performances and complexities of the analyzed architectures. Finally, in Section 6 we provide some concluding remarks.

2. State-of-the-art CNN architectures to detect P300

Convolutional Neural Networks (CNN) have become the state-of-the-art for single-trial P300 detection from EEG signals. Recently, many different CNN architectures have been proposed for this task, achieving high detection performances. This section gives a concise presentation of these architectures, specifying the minor modifications we made in some of them for comparison purposes. Details about the activation functions can be found in Appendix A.

CNN-1. Cecotti et al. [22] proposed a 4-layer architecture, named CNN-1. To the best of our knowledge, this was the first CNN for P300 detection. The first layer of CNN-1 is a 1D-convolution in the space domain, representing spatial filters. The second layer is a 1D-convolution over time which subsamples and filters the signals. Both convolutional layers have a Scaled Hyperbolic Tangent activation function. The output of the second convolutional layer is flattened and fed into a fully-connected layer with 100 neurons. Finally, the classification layer is composed of two Sigmoid neurons as output. Table B.1 shows further details about the CNN-1 architecture. Additionally, the authors presented the CNN-3, a CNN-1 architecture with one filter in its first 1D-convolutional layer, in contrast to the 10 filters of the CNN-1. See Table B.2 to compare the differences in the number of parameters and the outputs of the layers. To evaluate the performance of these architectures in the current research context, we slightly modified these two architectures as follows: *i*) we changed from two output neurons with a

Sigmoid activation function to two output neurons with a Softmax activation function and *ii*) we changed the loss function from Mean Square Error to Binary Cross Entropy. We named the modified CNN-1 as UCNN-1 and the CNN-3 as UCNN-3.

CNN-R. Manor and Geva [23] proposed a more complex architecture, containing two convolutional-max-pooling blocks, a convolutional layer, two fully connected layers, and a Softmax classification layer. The first convolutional block performs a spatial convolution. The weights and biases of this layer are regularized with a spatiotemporal penalty that reduces overfitting. The second convolutional block finds temporal patterns in the signal that represent the change in amplitude of the spatial maps learned in the first block. CNN-R uses a ReLU activation function in all its hidden layers and applies Dropout after each fully-connected layer. Table B.3 depicts the detailed CNN-R’s architecture.

DeepConvNet. Schirrmester et al. [16] proposed an architecture consisting of four convolutional blocks followed by a Softmax classification layer. The first convolutional block is composed of two layers: in the first layer each filter performs a convolution over time and in the second each filter performs a spatial filtering. The first convolutional block is followed by three standard convolutional-max-pooling blocks. DeepConvNet uses ELU as activation function in all its hidden layers and Dropout is applied after each convolutional block. Table B.4 shows further details about the architecture.

ShallowConvNet. In addition to the DeepConvNet, Schirrmester et al. [16] presented an architecture originally designed to decode band-power features. The first two layers perform a temporal convolution and a spatial filtering. They are followed by a squaring nonlinearity, an average pooling operation, a logarithmic activation function, and a Softmax classification layer. In ShallowConvNet, Dropout is applied before the Softmax classification layer. See Table B.5 for more details about the architecture.

BN³. Liu et al. [17] proposed a six-layer architecture that combines Batch Normalization [24] and Dropout [25] techniques that is less susceptible to overfitting and faster in training than CNN-1. First, it applies a 1D convolutional layer for spatial feature

extraction, followed by a 1D convolutional and a subsampling layer for temporal feature extraction. The two convolutional layers are followed by a Batch Normalization, two fully connected layers with 128 neurons and a classification layer with a single Sigmoid neuron. The ReLU activation function is used in the second convolutional layer and the Hyperbolic Tangent activation function is used in the two fully connected layers. Dropout is applied after each fully-connected layer. Table B.6 depicts details about the architecture.

EEGNet. Lawhern et al. [4] proposed a compact CNN architecture consisting of two convolutional blocks followed by a Softmax classification block. The first convolutional block decomposes the EEG signal at different band-pass frequencies and reduces the number of trainable parameters by a depthwise convolution. The architecture applies Batch Normalization [24] along the feature map dimension before applying the Exponential Linear Units nonlinearity. The second convolutional block uses a separable convolution, which is a depthwise convolution followed by point-wise convolutions, to reduce the number of parameters and to decouple the relationship of feature maps. EEGNet applies Average Pooling and Dropout after each convolutional block. See Table B.7 for more details about the architecture.

OCLNN. Shan et al. [26] proposed a one-convolutional-layer architecture which learns features directly from the raw temporal data instead of learning from abstract temporal data extracted through a spatial convolutional layer, as was frequently done in previous architectures. It is the simplest CNN-based architecture presented so far. It consists of a 1D convolutional block with a ReLU activation function, followed by a Softmax classification block. The convolutional block divides the temporal signals from the input channels into 15 parts and performs a convolution operation on each one for temporal and spatial feature extraction. Dropout is applied before the Softmax classification block. See Table B.8 for more details about the architecture.

3. Methods

As previously explained, we would like to provide an alternative to complex architectures for P300 detection. To that end, we now describe a simple CNN-based

architecture, the SepConv1D. Additionally, we describe a one-layer Fully-Connected Neural Network.

3.1. EEG signals

The EEG signals are recorded by C channels and discretized by S temporal signal samples. From now on, $S = T \times F$, where T corresponds to the time period between the moment posterior to the stimulus and T , and F denotes the signal sampling frequency. The filtered signals are represented by a matrix \mathbf{X} of size $C \times T$, where each vector $\mathbf{x}_c = [x_1, \dots, x_T]$ represents the signals recorded by a single EEG channel $c \in \{1, \dots, C\}$.

3.2. SepConv1D

SepConv1D is a simple CNN architecture consisting of two layers. The architecture is illustrated in Figure 1. The EEG input signals to the architecture is the matrix \mathbf{X}^T .

In the first layer, a depthwise separable 1D convolutional block is applied to the input signals to learn temporal features. The kernel size of the convolution operation is $16 \times C$. This kind of convolution has been successfully used before by the EEGNet architecture [4]. On the other hand, since input signals are acquired from all C electrodes, they provide information in the space domain. Thus, this layer learns features from both the temporal and spatial domains. We use a stride of eight for the convolution operation and a Hyperbolic Tangent Sigmoid activation function (see Appendix A). The number of filters in the convolutional layer was set through an experimental evaluation, which is described in Section 5. The classification of the EEG signal is done through a fully-connected layer, which is fed by the resulting vector of flattening the output of the convolutional layer. The fully-connected layer is defined as:

$$\mathbf{y}^{(1)} = f(\mathbf{w}^{(1)}\mathbf{y}^{(0)} + \mathbf{b}^{(1)}), \quad (1)$$

where $\mathbf{w}^{(1)}$ and $\mathbf{b}^{(1)}$ are the weights and biases, respectively. This layer is composed of a single neuron with a Sigmoid activation function (see Appendix A for the definition), which yields the P300 detection result as a binary classification output.

SepConv1D is based on OCLNN; the main difference between them is that SepConv1D uses a depthwise separable 1D convolutional layer to reduce the number of

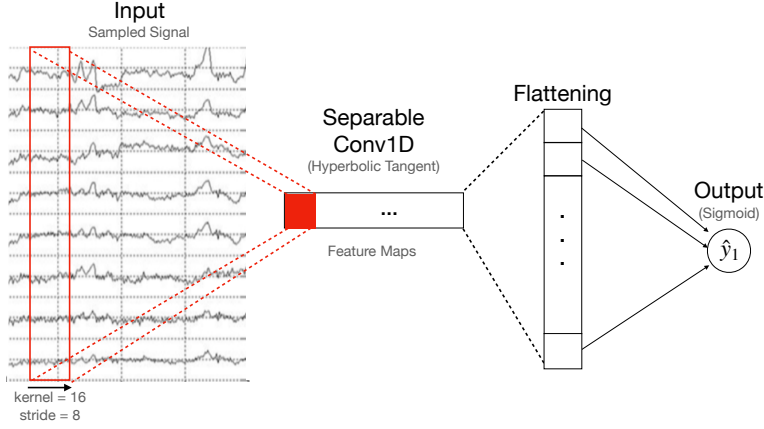


Figure 1: SepConv1D, a CNN architecture consisting of a depthwise separable 1D convolutional layer followed by a Sigmoid classification layer. Table 1 shows further details about the architecture.

trainable parameters, whereas OCLNN uses a standard 1D convolutional layer. Moreover, OCLNN connects two neurons to a Softmax function in the output layer and applies Dropout, while SepConv1D connects a single neuron to a Sigmoid function and does not apply Dropout. Table 1 details the number of filters, the input and output sizes of the layers, and the number of parameters.

3.3. FCNN

We also propose the use of a one-layer Fully-Connected Neural Network (FCNN), similar to the one presented by [11] (see Figure 2). We used the Hyperbolic Tangent activation function in the hidden layer and a Sigmoid function in the output layer (see Appendix A). The FCNN is composed of two neurons in the hidden layer, whose output is given by $h_j^{(1)} = f\left(\sum_{i=1}^D w_{ij}^{(0)} x_i + b_j^{(0)}\right)$, where $w_{ij}^{(0)}$ is the connection weight from input i in layer 0 to the intermediate neuron j , $b_j^{(0)}$ is the bias of the neuron j , x_i is an element of the vector resulting of flattening the matrix \mathbf{X} , and $D = C \cdot T$. Thus, the output of FCNN is $\hat{y}_1 = f\left(\sum_{j=1}^2 w_{j1}^{(1)} h_j^{(1)} + b^{(1)}\right)$, where $w_{j1}^{(1)}$ is the connection weight from neuron j in layer (1) to the output neuron and $b^{(1)}$ is the bias of the output neuron. See Table B.9 for more details about the architecture.

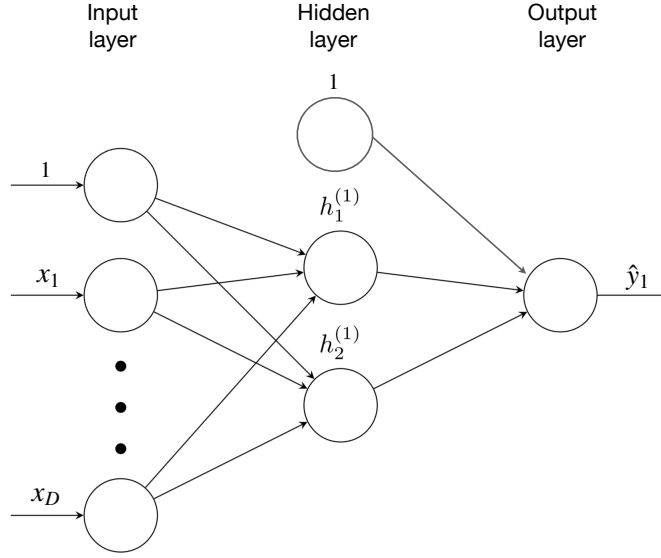


Figure 2: One-layer Fully-Connected Neural Network composed of an input, a two-neuron hidden layer, and an output layer.

4. Experimental Design

We compare the performance of the state-of-the-art CNN architectures with Sep-Conv1D and FCNN for both single-trial within-subject and cross-subject P300 detection. In what follows, we explain in detail the experimental design.

4.1. Datasets

For our experiments, we used four benchmark datasets where the subjects were visually stimulated with the Donchin 6×6 speller matrix described in [2]. The speller matrix is composed of alphanumeric symbols that allow the subjects to write a word. In all datasets, the presence of the P300 component in an EEG signal was indicated by $y = 1$ and the absence by $y = 0$.

P300-LINI [27]

This dataset is composed of the EEG signals of 22 healthy students from 21 to 25 years old without known neurological damage. The P300-LINI dataset contains signals of ten EEG channels (Fz, C4, Cz, C3, P4, Pz, P3, PO8, Oz, and PO7) and was acquired following the international 10-20 system, with the right earlobe and the right mastoid

serving as reference and ground locations respectively. However, we only used six of them (Fz, Cz, Pz, PO8, Oz, and PO7), since it has been previously reported [28] to be the most relevant to detect the P300 component. The signal was digitized at a rate of 256 Hz and processed online using a notch filter (Chebyshev of order 4) with cutoff frequencies between 58 and 62 Hz and a bandpass filter (Chebyshev of order 8) with cutoff frequencies between 0.1 and 60 Hz.

In order to generate the oddball paradigm, the rows and columns of the matrix flashed randomly 15 times every 125 ms (i.e., trials); each flash lasted 62.5 ms. The resulting set D_1 consists of 480 EEG signals that potentially contained P300 and 2,400 EEG signals without P300, for each subject. Each segment was filtered offline using a 4th-order Butterworth bandpass filter with bandwidth range from 0.1 to 12 Hz to extract the ERP signals embedded in the EEG. The DC component was removed by subtracting the mean of each electrode from the filtered signal. We extracted segments of 800 ms of EEG data after every stimulus. Finally, the linear trend was removed from each segment.

BCI Competitions

BCI Competition II - Data set Iib [29] and BCI Competition III - Data set II [30] contain 64 channels and were acquired following the international 10-10 system. The signals were digitized at a rate of 240 Hz and filtered with cutoff frequencies between 0.1 and 60 Hz. In order to generate the oddball paradigm, the rows and columns of the matrix flashed randomly 15 times every 100 ms, with an inter stimulus interval of 75 ms.

BCI Competition II - Data set Iib [29] is composed of the EEG signals of one subject collected in three sessions (sessions 10-12): session 10 has five runs, session 11 has six runs, and session 12 has eight runs. We only processed the labeled data of sessions 10 and 11. In every case, we extracted segments of 650 ms of EEG data after every stimulus. The resulting set D_2 consists of 570 EEG signals that potentially contained P300 and 2,850 EEG signals without P300.

BCI Competition III - Data set II [30] is composed of the EEG signals of two subjects. Each subject generated a training and a test set. We processed the training

sets of both subjects since they are labeled. We extracted segments of 1000 ms of EEG data after every stimulus. The resulting set D_3 consists of 3,825 EEG signals that potentially contained P300 and 12,750 EEG signals without P300, for each subject.

BNCI Horizon 2020

Dataset 8. P300 speller with ALS patients was acquired by Riccio et al. [31] and its available at [32]. This dataset is composed of the EEG signals of eight subjects with Amyotrophic Lateral Sclerosis. This dataset contains eight EEG channels (Fz, Cz, Pz, Oz, P4, P3, PO8, and PO7) and was acquired following the international 10-10 system. All channels were referenced to the right earlobe and grounded to the left mastoid. The signal was digitized at a rate of 256 Hz and band-pass filtered with cutoff frequencies between 0.1 and 30 Hz. In order to generate the oddball paradigm, the rows and columns of the matrix flashed randomly 10 times at a rate of 4 Hz for 125 ms, with an inter stimulus interval of 125 ms. We extracted segments of 800 ms of EEG data after every stimulus. The resulting set D_4 consists of 700 EEG signals that potentially contained P300 and 3,500 EEG signals without P300, for each subject.

4.2. Evaluation

For the architectures under analysis, we ran 200 training iterations (epochs) of the Adam optimizer with the parameters recommended by [33] and performed early stopping if the validation loss did not improve in 50 iterations. Categorical Cross-Entropy was the loss function for all architectures except for BN^3 , FCNN, and SepConv1D for which the Binary Cross Entropy loss function was used, and for CNN1 and CNN3 which used Mean Squared Error. The Glorot uniform initializer was employed for all architectures except for CNN1, UCNN1, CNN3 and UCNN3, which employed the initializer proposed by Cecotti and Gräser [22]. In addition, we applied standarization on each EEG channel separately.

For within-subject detection, we performed 10 repetitions of stratified 5-fold cross-validation for every subject. In each repetition 5 splits were generated using 5-fold cross-validation, where a split consisted of a training set with 80% of the data of a given subject and a validation set with the remaining 20%. For cross-subject detection,

we used data from a subset of subjects to train a model for another subject. Consequently, the evaluation of this type of detection was only possible on the D_1 and D_4 datasets, because the D_2 and D_3 datasets have only 1 and 2 subjects respectively. For this evaluation, we performed a leave-two-out cross-validation, where one subject is selected for testing, another for validation, and the remaining for training. This process was repeated for each subject, producing 22 folds for D_1 and 8 folds for D_4 . For both types of detection, we computed the Area Under the Curve (AUC) of the Receiver Operating Characteristic (ROC) over the test set in each split.

4.3. Implementation details

The experiments were performed on a single PC with Linux Ubuntu 16.04, an Intel(R) Core(TM) i7-6700K CPU @ 4.00GHz, 64 GB in RAM, and an NVIDIA GeForce GTX 1080 GPU with 2560 CUDA cores and 8 GB of RAM. The architectures were implemented in Keras [34] with Tensorflow 1.14.0 [35] as backend. For DeepConvNet, ShallowConvNet and EEGNet, we used the code provided by Lawhern et al.: <https://github.com/vlawhern/arl-eegmodels>. The rest of the architectures were implemented following the descriptions of the corresponding papers. The code of all the architectures under analysis is available at <http://github.com/gibranfp/P300-CNNT>

5. Results and Discussion

5.1. Within-subject classification

In this section, we describe the experiments for within-subject P300 detection. These experiments were performed on the four benchmark datasets described in Section 4.1.

5.1.1. Selection of the number of filters for the SepConv1D

In order to find the balance between computational cost and performance, we evaluated SepConv1D with 1, 2, 4, 8, 16 and 32 filters. Figure 3 shows the mean and standard deviation of the AUC values obtained over all repetitions, splits and subjects for SepConv1D with the different number of filters on the four benchmark datasets. For

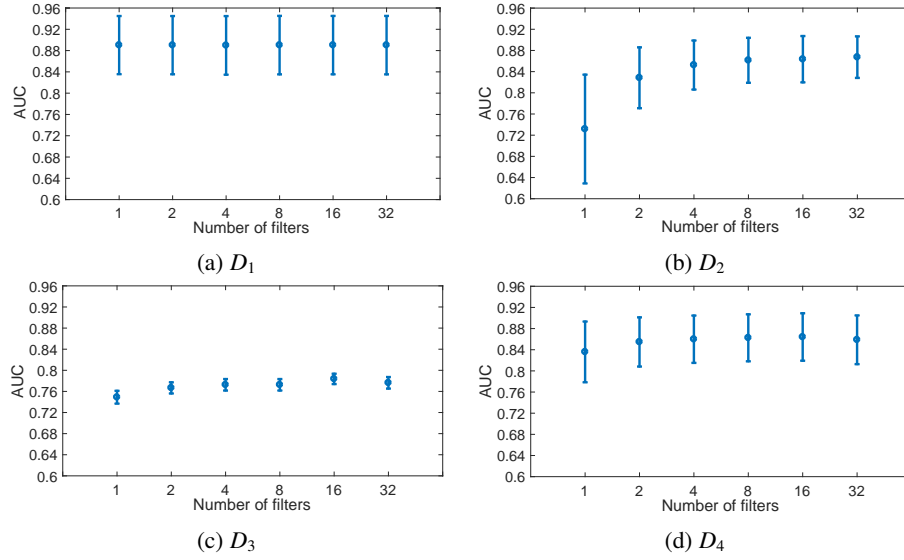


Figure 3: Comparison of SepConv1D mean AUC with different number of filters for within-subject P300 detection.

Layer	No. filters	Size	No. params	Output	Activation function	Options
Input		206×6				
ZeroPadding1D	4			$(214, 6)$		
SeparableConv1D	4	kernel = 16, stride = 8	124	$(25, 4)$		padding = 4
Activation				$(25, 4)$	\tanh	
Flatten				(25)		
Dense	1		101	(1)	Sigmoid	

Table 1: SepConv1D architecture for within-subject classification with four filters for dataset D_1 (see Section 4.1).

D_1 the performance is almost identical in all cases, while for D_2 and D_4 the peak performance is reached with four and eight filters and remains relatively stable with larger filter numbers. For D_3 the highest mean AUC is achieved with 16 filters, although it is very similar with 4, 8, and 32 filters and just slightly lower with 1 and 2 filters. Given these results, it would be possible to select only one filter for D_1 and 16 filters for D_3 . However, four filters appears to be adequate for all datasets. Thus, we decided to use SepConv1D with four filters for subsequent experiments; the amount of trainable parameters for this configuration is as follows (see Table 4): 225 for D_1 , 1,361 for D_2 , 1,405 for D_3 , and 265 for D_4 . See Table 1 for more details about the SepConv1D architecture with four filters and EEG signals of six channels and 206 samples as input.

Architecture	D_1	D_2	D_3	D_4
CNN1	0.89±0.06	0.88±0.04	0.82±0.04	0.85±0.05
UCNN1	0.88±0.07	0.87±0.08	0.81±0.05	0.85±0.05
CNN3	0.72±0.16	0.78±0.14	0.68±0.13	0.66±0.14
UCNN3	0.77±0.13	0.81±0.09	0.7±0.11	0.71±0.13
CNNR	0.88±0.06	0.86±0.05	0.76±0.06	0.86±0.04
DeepConvNet	0.9±0.05	0.9±0.04	0.84±0.04	0.88±0.04
ShallowConvNet	0.83±0.08	0.82±0.07	0.78±0.05	0.86±0.05
BN ³	0.88±0.06	0.81±0.05	0.8±0.05	0.84±0.05
EEGNet	0.89±0.05	0.9±0.04	0.83±0.04	0.88±0.04
OCLNN	0.89±0.05	0.85±0.05	0.8±0.05	0.85±0.05
FCNN	0.89±0.05	0.78±0.05	0.75±0.04	0.84±0.05
SepConv1D	0.88±0.06	0.85±0.05	0.82±0.04	0.86±0.05

Table 2: Mean AUC and standard deviation obtained by the architectures under analysis for within-subject single-trial P300 detection on all datasets. See details in tables C.1-C.4.

5.1.2. Comparison with state-of-the-art CNN-based architectures

Table 2 compares the performance of SepConv1D and FCNN with state-of-the-art CNN architectures for within-subject P300 detection on the four benchmark datasets. The mean and standard deviation of the AUC values obtained over all repetitions, splits and subjects are reported for each architecture and dataset.

We performed statistical testing using a one-way analysis of variance (ANOVA) between the architectures under analysis. Then, we performed a multiple comparison of the AUC values. The results are shown in Figure 4. As can be seen, the AUC values obtained by SepConv1D are close to those obtained by the best performing architectures on all datasets. Figures 4(b), (c), and (d) show that DeepConvNet and EEGNet achieved the best performance in all datasets. However, the difference between SepConv1D and EEGnet is not statistically significant for D_1 and D_3 . Also, CNN1 is better than SepConv1D and their difference is statistically significant only for D_2 . In all cases, the differences between UCNN1, OCLNN, and SepConv1D are not statistically significant. In all cases, CNN3 and UCNN3 had the lowest AUC values. Additionally, FCNN performs worse than sepConv1D except for D_1 .

5.2. Cross-subject P300 detection

We now proceed to describe the experiments for cross-subject P300 detection. These experiments were performed only on datasets D_1 and D_4 because datasets D_2

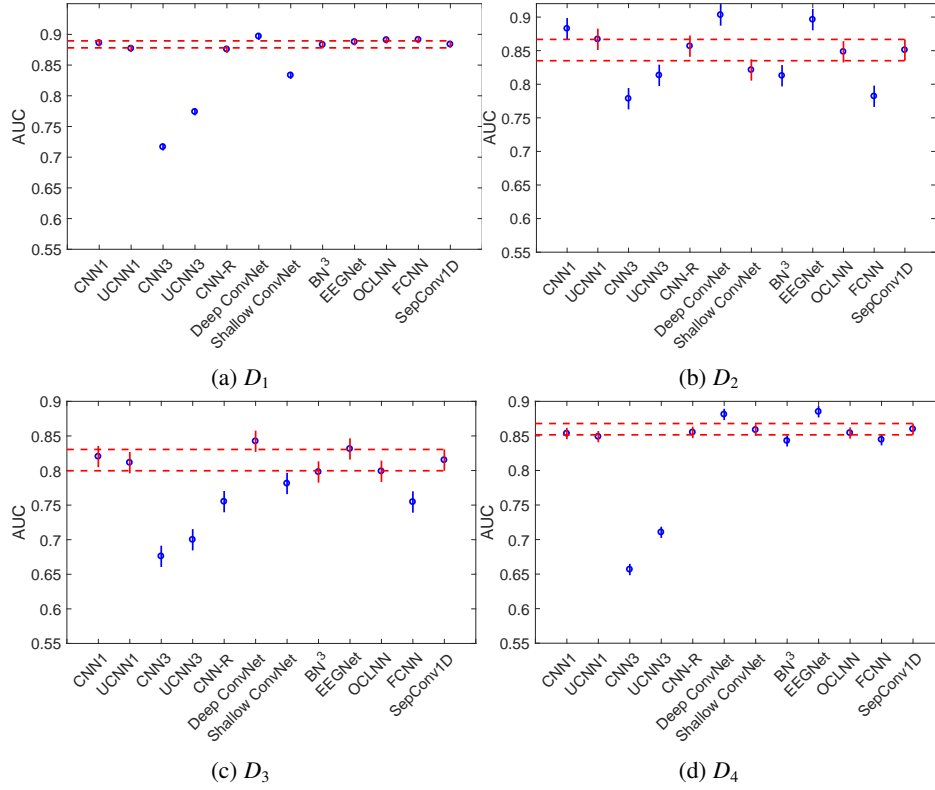


Figure 4: Multiple comparison of the AUC values obtained by SepConv1D and state-of-the-art CNN architectures for within-subject P300 detection on the four benchmark datasets.

and D_3 had only one and two subjects respectively.

5.2.1. Selection of the number of filters for the SepConv1D

As in within-subject P300 detection, we carried out experiments with 1, 2, 4, 8, 16 and 32 filters for SepConv1D to find a compromise between computational cost and performance for cross-subject P300 detection. Figure 5 shows the mean AUC and standard deviation for both datasets. Interestingly, the mean AUC and the standard deviation are very similar for all the filters on dataset D_1 . Similarly, only a slightly better performance on D_4 was obtained with one and two filters. Thus, we decided to use four filters for subsequent experiments for datasets D_1 and D_4 .

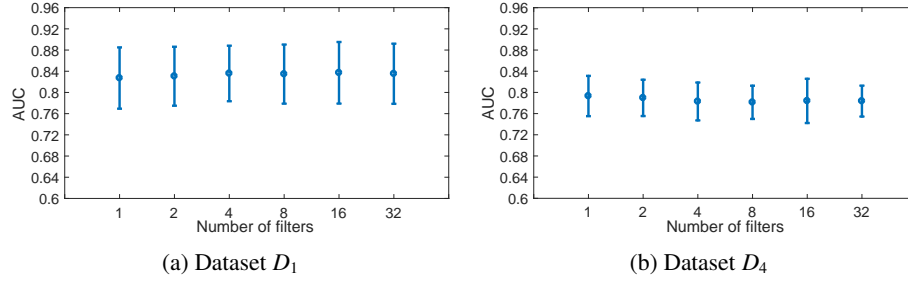


Figure 5: Comparison of mean AUC values obtained by SepConv1D with different number of filters for cross-subject P300 detection on datasets (a) D_1 and (b) D_4 .

Architecture	D_1	D_4
CNN1	0.82 ± 0.05	0.78 ± 0.04
UCNN1	0.84 ± 0.06	0.78 ± 0.05
CNN3	0.78 ± 0.11	0.73 ± 0.08
UCNN3	0.83 ± 0.06	0.76 ± 0.07
CNN-R	0.83 ± 0.06	0.79 ± 0.04
DeepConvNet	0.84 ± 0.06	0.79 ± 0.04
ShallowConvNet	0.82 ± 0.07	0.79 ± 0.03
BN ³	0.83 ± 0.06	0.78 ± 0.04
EEGNet	0.84 ± 0.06	0.8 ± 0.03
OCLNN	0.83 ± 0.06	0.79 ± 0.04
FCNN	0.83 ± 0.06	0.75 ± 0.04
SepConv1D	0.84 ± 0.06	0.78 ± 0.04

Table 3: Mean AUC and standard deviation obtained by the architectures under analysis for single-trial cross-subject P300 detection on D_1 and D_4 . See details in tables C.2 and C.4.

5.2.2. Comparison with state-of-the-art CNN-based architectures

Table 3 presents the performance of all architectures for cross-subject P300 detection on datasets D_1 and D_4 . The mean and standard deviation of the AUC values obtained over all splits are reported for each architecture (see details in tables C.2 and C.4).

We also performed an ANOVA statistical testing between the architectures under analysis, as well as a multiple comparison of their AUC values. The results can be seen in Figure 6. The comparison shows very similar performances between all the architectures, except for CNN3, that has the worst performance in all cases. However, only on D_4 EEGNet has the best performance among all the architectures and it is statistically different from SepConv1D ($p > 0.05$).

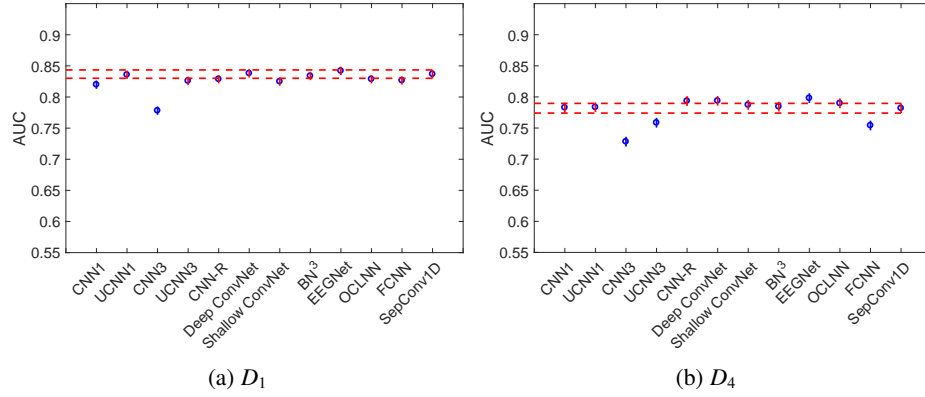


Figure 6: Multiple comparison of the AUC values obtained by SepConv1D and state-of-the-art CNN architectures for cross-subject P300 detection on D_1 and D_4 .

Architecture	D_1	D_2	D_3	D_4
CNN-1/UCNN-1	1,036,922	787,502	1,207,502	1,036,942
CNN-3/UCNN-3	1,031,009	781,067	1,201,067	1,031,011
CNN-R	19,848,098	16,445,794	21,950,818	19,848,290
DeepConvNet	139,877	174,927	176,927	141,127
ShallowConvNet	12,082	104,322	105,282	15,282
BN ³	44,589	39,489	47,681	44,625
OCLNN	1,842	11,762	16,882	2,290
EEGNet	1,394	2,258	2,354	1,426
FCNN	2,477	19,973	30,725	3,301
SepConv1D	225	1,361	1,405	265

Table 4: Number of trainable parameters of each architecture for all datasets.

5.3. Complexity

Table 4 details the number of trainable parameters used by each architecture for the benchmark datasets. In general, the number of parameters has been decreasing since CNNs were first introduced for P300 detection in 2011 by Cecotti and Graser [22]. It is worth noting that OCLNN, EEGNet, FCNN, and SepConv1D are able to reduce the number of parameters to the order of thousands, at least in one of the datasets (see Figure 7(a)). However, OCLNN requires more than 14,700 parameters for datasets D_2 and D_3 . Something similar occurs with FCNN, which uses almost 20,000 parameters for D_2 . In contrast, EEGNet manages to keep the number of parameters more or less stable and in the order of thousands. In all cases, SepConv1D requires the least number of parameters: as few as 225 and 265 parameters for datasets D_1 and D_4 respectively and at most 1,361 and 1,405 for datasets D_2 and D_3 respectively.

On the other hand, Figure 7(b) takes a closer look at the complexity of EEGNet and

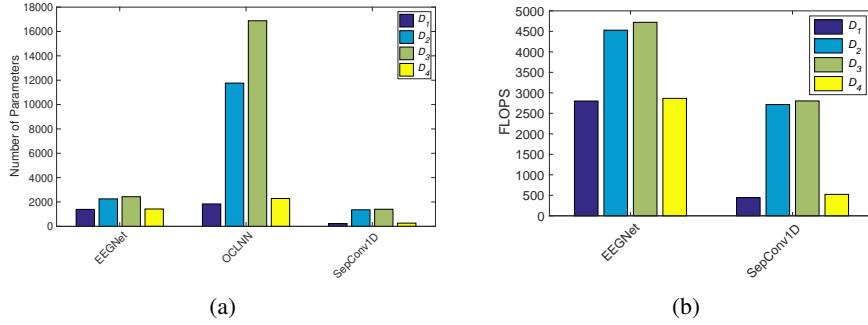


Figure 7: A comparison of the architectures’ complexity for each dataset: (a) trainable parameters and (b) FLOPS = Floating Point Operations per Second. For more details see tables 4 and C.5, respectively.

SepConv1D in terms of FLOPS. As previously mentioned, the differences between the AUC values of SepConv1D and those of EEGNet are not statistically significant on dataset D_1 . However, the number of FLOPS and trainable parameters needed by SepConv1D is significantly lower compared to EEGNet. As previously explained, the differences between the AUC values of EEGNet and SepConv1D are statistically significant for within-subject P300 detection on datasets D_2 and D_4 . Specifically, EEGNet obtained a 0.05 and 0.04 higher mean AUC but at the cost of 1,814 and 2,342 additional FLOPS and 897 and 1,161 additional parameters, respectively. Something similar happens for dataset D_3 , even though the difference between SepConv1D and EEGNet is not statistically significant.

Finally, we analyzed the training time and the number of epochs needed to meet the early stopping criteria as well as the inference time (i.e., the time needed to process the test set) for the architectures under analysis (see Table 5). To illustrate the performance of the architectures, we compared their mean AUC with both their corresponding epochs (Figure 8(a)) and inference time (Figure 8(b)) for within-subject P300 detection on the dataset D_3 . The differences in time between SepConv1D and the architectures with the highest mean AUC (EEGNet and DeepConvNet) are 0.09 and 0.15 seconds respectively, while the differences in the number of epochs are 84.49 and 31.4 respectively. These differences are significantly higher than the number of epochs and inference time required by SepConv1D, even though the differences between their AUC values were not statistically significant.

Architecture		D_1	D_2	D_3	D_4
CNN1	E	97±33	68± 8	65± 6	71±14
	TT	5.33±1.74	8.08± 1.39	59.66± 9.6	5.79±1.29
	IT	0.04±0.004	0.06 ±0.013	0.24± 0.015	0.05± 0.006
UCNN1	E	88±27	74±26	66±12	76±24
	TT	4.89±1.46	8.8± 3.01	63.93± 15.76	6.27±1.98
	IT	0.04±0.004	0.06 ±0.013	0.24± 0.014	0.05± 0.006
CNN3	E	111±37	86±28	85±29	93±31
	TT	5.25±1.75	9.68± 3.28	76.1± 28.19	6.56±2.13
	IT	0.04±0.003	0.06 ±0.01	0.24± 0.013	0.05± 0.004
UCNN3	E	114±42	78±13	72±16	87±30
	TT	5.41±1.97	9.01± 1.84	68.42± 20.46	5.87±1.93
	IT	0.04±0.003	0.06 ±0.009	0.24± 0.011	0.05± 0.004
CNN-R	E	61± 2	167±29	89±29	64± 2
	TT	12.46±0.49	47.25± 6.57	148.38± 45.75	18.68±0.67
	IT	0.07±0.01	0.09 ±0.026	0.32± 0.026	0.09± 0.014
DeepConvNet	E	122±40	79±10	122±25	106±24
	TT	13.33±4.15	26.41± 2.88	276.22± 58.13	18.16±3.97
	IT	0.11±0.007	0.13 ±0.013	0.37± 0.013	0.12± 0.010
ShallowConvNet	E	177±29	144±45	95±40	157±33
	TT	16.57±2.69	63.41±18.85	281.23±116.77	25.12±5.29
	IT	0.06±0.011	0.09 ±0.015	0.37± 0.018	0.06± 0.010
BN ³	E	113±21	77± 4	71± 3	95± 9
	TT	4.04± 0.7	8.8± 1.31	71.08± 10.78	5.06±0.56
	IT	0.07±0.001	0.09 ± 0.007	0.27± 0.009	0.08± 0.002
EEGNet	E	200± 3	166±30	175±30	198± 7
	TT	17.18± 0.5	53.69± 7.28	360.66± 62.81	27.67±1.13
	IT	0.08±0.005	0.10 ± 0.005	0.31± 0.008	0.09± 0.005
OCLNN	E	199± 5	129±41	87±11	161±26
	TT	4.55±0.28	11.88± 2.84	75.69± 17.95	5.87±0.99
	IT	0.04±0.002	0.05 ± 0.003	0.22± 0.005	0.04± 0.002
FCNN	E	197± 7	89±21	98±11	132±12
	TT	3.74±0.21	5.71± 1.26	53.88± 7.23	4.04±0.38
	IT	0.02±0.001	0.04±0.002	0.17± 0.014	0.03± 0.001
SepConv1D	E	199± 5	104±14	90±12	183±24
	TT	5.34±0.32	10.61± 2.01	80.02± 14.7	8.22±1.14
	IT	0.03±0.002	0.05 ±0.003	0.22± 0.009	0.04± 0.002

Table 5: Epochs (E), train time (TT), and inference time (IT) obtained by the architectures under analysis for single-trial within-subject P300 detection on each dataset.

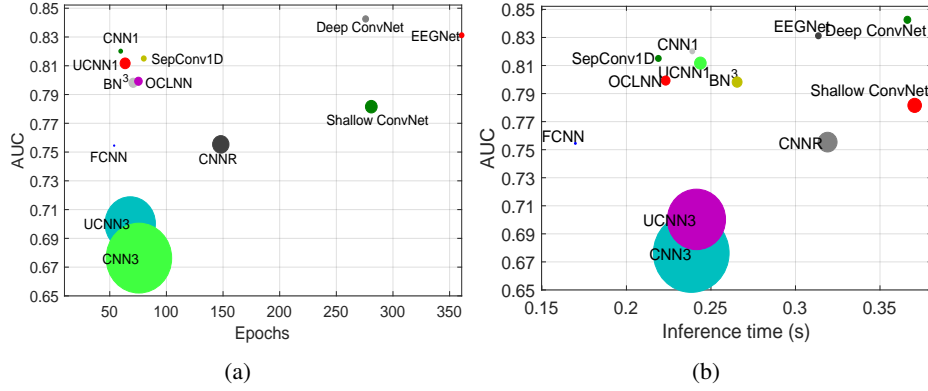


Figure 8: Comparison between mean AUC values and both (a) epochs and (b) inference time (see Table 5), obtained by the architectures under analysis for within-subject P300 detection on D_3 . The standard deviations of the AUC are directly proportional to the diameter of the circles.

6. Conclusions

In this paper, we presented SepConv1D, a simple Convolutional Neural Network architecture consisting of a depthwise separable 1D convolutional layer followed by a Sigmoid classification layer. The proposed architecture can perform within-subject and cross-subject single-trial P300 detection on a par with state-of-the-art CNN-based architectures but with a lower computational cost. We showed experimentally that deep and complex neural network does not necessarily achieve better performance in P300 detection from EEG signals.

In all cases, SepConv1D required the lowest number of trainable parameters and FLOPS, and only the FCNN has a lower inference time, although it has a worst performance. In the dataset with the largest number of subjects, it only required 225 parameters, while EEGNet (the architecture with the closest number of parameters) required 1,474, even though their performance was not significantly different. Additionally, the number of FLOPS and inference time required by SepConv1D were significantly lower: EEGNet required 2,801 FLOPS and 0.000274 ms of inference time, while SepConv1D required only 443 FLOPS and less than a half of inference time.

The performance difference between EEGNet and SepConv1D was statistically significant for within-subject P300 detection on two datasets, where EEGNet obtained a 0.05 and 0.04 higher mean AUC but requires 1,814 and 2,342 more FLOPS and 897

and 1,161 additional parameters and takes 0.05 more seconds for inference. Moreover, we analyzed the time and the number of epochs needed for the architectures under analysis to meet the early stopping criteria during training. Moreover, among the top performing architectures (i.e., EEGNet and DeepConvNet), SepConv1D required the least training time. For cross-subject P300 detection, there were no statistically significant differences in performance between the architectures on any of the datasets. These findings are important because simpler, cheaper, faster, and more portable Brain Computer interfaces can be built.

7. Acknowledgment

This work was supported by UNAM through the PAPIIT grant IA104016 and by the PRODEP-SEP grant 2017 for the project "Interfaces Brain Computer with perspectives to its application in service robots".

Appendix A. Activation Functions

In this appendix, we describe the activation functions used by the analyzed architectures.

- The Linear activation function is a polynomial of one degree, which is limited in its learning power of complex functional mappings. It is defined as

$$f(z_i^{(l)}) = \gamma z_i^{(l)}, \quad (\text{A.1})$$

where γ is the slope.

- The *Log* activation function is a logarithmic function bounded in a range of $[1e-7, 10000]$.

$$f(z_i^{(l)}) = \log(z_i^{(l)}). \quad (\text{A.2})$$

- The Square activation function does not have a stable range since they explode in magnitude quickly. Since its output is a big value, this function tends to result in bad generalization. Additionally, it takes longer to converge than other activation functions. It is defined as

$$f(z_i^{(l)}) = z_i^{(l)2}. \quad (\text{A.3})$$

- The Sigmoid activation function is a sigmoidal function in the range $[0, 1]$. It is defined as

$$f(z_i^{(l)}) = \frac{1}{1 + e^{-z_i^{(l)}}}. \quad (\text{A.4})$$

- The Hyperbolic Tangent activation function (\tanh) is a sigmoidal function in the range $[-1, 1]$. It is defined as

$$f(z_i^{(l)}) = \tanh(z_i^{(l)}) = \frac{e^{2z_i^{(l)}} - 1}{e^{2z_i^{(l)}} + 1}. \quad (\text{A.5})$$

- The Scaled Hyperbolic Tangent activation function (stanh) [36] is a sigmoidal function in the range $[-1, 1]$ whose advantage is that the negative inputs will be mapped strongly negative and the zero inputs will be mapped near zero. It is defined as

$$f(z_i^{(l)}) = 1.7159 \tanh\left(\frac{2}{3} z_i^{(l)}\right). \quad (\text{A.6})$$

- The Softmax activation function [37] turns scores into probabilities that sum to one. It is defined as

$$f(z_i^{(l)}) = \frac{e^{z_i^{(l)}}}{\sum_j e^{z_j^{(l)}}}. \quad (\text{A.7})$$

- The Rectified Linear Unity (ReLU) alleviates the vanishing and exploding gradient problems in deep neural networks that are usually associated with saturated activation functions such as Sigmoid or \tanh . The activation function rectifies the inputs \mathbf{z} by setting the negative values to zero and by keeping the positive values [38], which enables faster convergence during training:

$$f(z_i^{(l)}) = \max(0, z_i^{(l)}). \quad (\text{A.8})$$

- As with ReLU, the Exponential Linear Units (ELU) [39] alleviate the vanishing and exploiting gradient problems via the identity for positive values. They have negative values allowing them to push the mean of the activations closer to zero:

$$f(z_i^{(l)}) = \begin{cases} z_i^{(l)} & \text{if } z_i^{(l)} > 0 \\ \phi(e^{z_i^{(l)}} - 1) & \text{if } z_i^{(l)} \leq 0 \end{cases}. \quad (\text{A.9})$$

The ELU hyperparameter ϕ controls the value to which an ELU saturates for negative inputs.

Appendix B. Architectures

This appendix provides the specifications of the state-of-the-art CNN architectures analyzed in this paper. For the sake of simplicity, the reported number of filters, input size, number of parameters, and output size of every layer correspond only to those obtained for dataset D_1 .

Layer	No. filters	Size	No. params	Output	Activation function	Options
Input		206×6				
Conv1D	10	1	70	(206, 10)		padding = same, data format = "Channels last", bias and kernel initializer = **
Activation				(206, 10)	<i>stanh</i>	
Conv1D	50	13	6,550	(206, 50)		padding = same, data format = "Channels first", bias and kernel initializer = **
Activation				(206, 50)	<i>stanh</i>	
Flatten				(10, 300)		
Dense	100		1,030, 100	(100)	Sigmoid	
Dense	2		202	(2)	Sigmoid ¹ / Softmax ²	

Table B.1: CNN-1 and UCNN-1 architectures. ¹ CNN-1 uses Sigmoid activation. ² UCNN-1 uses Softmax activation.

Layer	No. filters	Size	No. params	Output	Activation function	Options
Input		206×6				
Conv1D	1	1	7	(206, 1)		padding = same, data format = "Channels last", bias and kernel initializer = **
Activation				(206, 1)	<i>stanh</i>	
Conv1D	50	13	700	(206, 50)		padding = same, data format = "Channels last", bias and kernel initializer = **
Activation				(206, 50)	<i>stanh</i>	
Flatten				(10, 300)		
Dense	100		1,030, 100	(100)	Sigmoid	
Dense	2		202	(2)	Sigmoid ¹ / Softmax ²	

Table B.2: CNN-3 and UCNN-3 architectures. ¹ CNN-3 uses Sigmoid activation. ² UCNN-3 uses Softmax activation.

Layer	No. filters	Size	No. params	Output	Activation function	Options
Input		206×6				
Conv1D	96	1	672	(206, 96)		activity regularizer ¹
Activation				(206, 96)	ReLU	
Max Pooling 1D	3	stride 2		(102, 96)		
Conv1D	128	6	73,856	(97, 128)		ReLU
Activation				(97, 128)	ReLU	
Max Pooling 1D	3	stride 2		(48, 128)		
Conv1D	128	6	98,432	(43, 128)		ReLU
Activation				(43, 128)	ReLU	
Flatten				(5, 504)		
Dense	2,048		11,274, 240	(2, 048)	ReLU	$p = 0.8$
Dropout				(2, 048)		
Dense	4,096		8,392,704	(4, 096)	ReLU	$p = 0.8$
Dropout				(4, 096)		
Dense	2		8,194	(2)		
Activation				(2)	Softmax	

Table B.3: CNN-R architecture. ¹ Activity regularizer = $0.01 \sum_{t=1}^{N-1} (a_{t+1}^{(l)} - a_t^{(l)})^2$, where $a_t^{(l)}$ is the output of the convolutional layer l at time t .

Layer	No. filters	Size	No. params	Output	Activation function	Options
Input		6×206				
Reshape		$1 \times 6 \times 206$				
Conv2D	25	1×5	150	(25, 6, 202)		max norm = 2
Conv2D	25	6×1	40,025	(25, 1, 202)		max norm = 2
BatchNorm			100	(25, 1, 202)		data format = "Channels first", $\epsilon = 1 \times 10^{-05}$, momentum = 0.1
Activation				(25, 1, 202)	ELU	
MaxPool2D		1×2 pool size and stride		(25, 1, 101)		
Dropout				(25, 1, 101)		$p = 0.5$
Conv2D	50	1×5	6,300	(50, 1, 97)		max norm = 2
BatchNorm			200	(50, 1, 97)		data format = "Channels first", $\epsilon = 1 \times 10^{-05}$, momentum = 0.1
Activation				(50, 1, 97)	ELU	
MaxPool2D		1×2 pool size and stride		(50, 1, 48)		
Dropout				(50, 1, 48)		$p = 0.5$
Conv2D	100	1×5	25,100	(100, 1, 44)		max norm = 2
BatchNorm			400	(100, 1, 44)		data format = "Channels first", $\epsilon = 1 \times 10^{-05}$, momentum = 0.1
Activation				(100, 1, 44)	ELU	
MaxPool2D		1×2 pool size and stride		(100, 1, 22)		
Dropout				(100, 1, 22)		$p = 0.5$
Conv2D	200	1×5	100,200	(200, 1, 18)		max norm = 2
BatchNorm			800	(200, 1, 18)		data format = "Channels first", $\epsilon = 1 \times 10^{-05}$, momentum = 0.1
Activation				(200, 1, 18)	ELU	
MaxPool2D		1×2 pool size and stride		(200, 1, 9)		
Dropout				(200, 1, 9)		$p = 0.5$
Flatten				(1, 800)		
Dense	2		4,802	(2)	Softmax	max norm = 0.5

Table B.4: DeepConvNet architecture. Version modified by [4].

Layer	No. filters	Size	No. params	Output	Activation function	Options
Input Reshape		6×206 $1 \times 6 \times 206$				
Conv2D	40	1×13	560	(40, 6, 194)		
Conv2D	40	6×1	9,600	(40, 1, 194)		
BatchNorm			160	(40, 1, 194)		
Activation AveragePool2D		pool 1×35 , stride 1×7		(40, 1, 194) (40, 1, 23)	Square	max norm constraint function = 2 max norm constraint function = 2, doesn't use bias axis to be normalized = 1, $\epsilon = 1 \times 10^{-05}$, momentum = 0.1
Activation Dropout Flatten				(40, 1, 23) (40, 1, 23) (900)	Log	$p = 0.5$
Dense	2		1,842	(2)	Softmax	max norm constraint function = 0.5

Table B.5: ShallowConvNet architecture. Version modified by [4].

Layer	No. filters	Size	No. params	Output	Activation function	Options
Input		206×6				
BatchNorm			24	206 × 6		
Conv1D	16	1	112	206 × 16	ReLU	bias initializer = Glorot Uniform bias initializer = Glorot Uniform, strides = 20, padding = same
Conv1D	16	20	5,136	11 × 16	ReLU	
BatchNorm			64	11 × 16		
Activation				11 × 16	ReLU	
Flatten				176		
Dense		128	22,656	128	<i>tanh</i>	bias initializer = Glorot Uniform $p = 0.8$
Dropout				128		
Dense		128	16,512	128	<i>tanh</i>	bias initializer = Glorot Uniform $p = 0.8$
Dropout				128		
Dense	1		129	1	Sigmoid	bias initializer = Glorot Uniform

Table B.6: BN³ architecture.

Appendix C. Per-subject mean AUC values and architecture complexities

References

- [1] J. Wolpaw, N. Birbaumer, W. J. Heetderks, D. J. McFarland, P. H. Peckham, G. Schalk, E. Donchin, L. A. Quatrano, C. J. Robinson, T. M. Vaughan, Brain-computer interface technology: A review of the first international meeting, IEEE Transactions on Rehabilitation Engineering 8 (2) (2000) 164–173.
- [2] E. Donchin, K. M. Spencer, R. Wijesinghe, The mental prosthesis: assessing the speed of a P300-based Brain-Computer Interface, IEEE transactions on rehabilitation engineering 8 (2) (2000) 174–179.
- [3] N. E. L. da Silva F, Electroencephalography: Basic Principles, Clinical Applications, and Related Fields, 5th Edition, Lippincott Williams & Wilkins, 2005.
- [4] V. J. Lawhern, A. J. Solon, N. R. Waytowich, S. M. Gordon, C. P. Hung, B. J. Lance, EEGNet: A compact convolutional network for EEG-based Brain-Computer Interfaces, Journal of Neural Engineering 15 (5) (2018) 056013.
- [5] R. Ramele, A. J. Villar, J. M. Santos, EEG Waveform analysis of P300 ERP with applications to Brain Computer Interfaces, Brain Sciences 8 (11).

Layer	No. filters	Size	No. params	Output	Activation function	Options
Input		6×206				
Reshape				$1 \times 6 \times 206$		
Conv2D	8	1×64	512	(4, 6, 206)	Linear	padding = same, doesn't use bias
BatchNorm			16	(4, 6, 206)		
DepthwiseConv2D		6×1	48	(8, 1, 206)	Linear	doesn't use bias, number of depth-wise convolution output channels = 2, max norm constraint function = 1
BatchNorm			32	(8, 1, 206)		
Activation				(8, 1, 206)	ELU	
AveragePool2D		1×4		(8, 1, 51)		p
Dropout				(8, 1, 51)		
SeparableConv2D	16	1×16	192	(8, 1, 51)	Linear	padding = same, doesn't use bias
BatchNorm			32	(8, 1, 51)		
Activation				(8, 1, 51)	ELU	
AveragePool2D		1×8		(8, 1, 6)		p
Dropout				(8, 1, 6)		
Flatten				(48)		
Dense	2		98	(2)	Softmax	max norm constraint regularization = 0.25

Table B.7: EEGNet architecture, where $p = 0.25$ or 0.5 (for cross-subject or within-subject classification, respectively). Adapted from [4].

Layer	No. filters	Size	No. params	Output	Activation function	Options
Input		206×6				
ZeroPadding1D						
Conv1D	16	kernel and stride = 14	1,360	(210, 6)		padding = 2
Activation				(15, 16)	ReLU	kernel and bias regularizer use L2 = 0.01
Dropout				(15, 16)		$p = 0.25$
Flatten				(240)		
Dense	2		482	(2)		
Activation				(2)	Softmax	

Table B.8: OCLNN architecture.

Layer	No. filters	No. params	Output	Activation function
Input			6×206	
Reshape			1236×1	
Dense	2	2,474	(2)	\tanh
Flatten			(2)	
Dense	1	3	(1)	Sigmoid

Table B.9: FCNN architecture.

- [6] F. Lotte, L. Bougrain, A. Cichocki, M. Clerc, M. Congedo, A. Rakotomamonjy, F. Yger, A review of classification algorithms for EEG-based Brain-Computer Interfaces: a 10 year update, Journal of Neural Engineering 15 (3) (2018) 031005.
- [7] D. J. Krusienski, E. W. Sellers, F. Cabestaing, S. Bayouth, D. J. McFarland, T. M.

- Vaughan, J. R. Wolpaw, A comparison of classification techniques for the P300 speller, *Journal of Neural Engineering* 3 (4) (2006) 299.
- [8] Y. Atum, I. Gareis, G. Gentiletti, R. Acevedo, L. Rufiner, Genetic feature selection to optimally detect P300 in Brain Computer Interfaces, in: *Engineering in Medicine and Biology Society (EMBC), 2010 Annual International Conference of the IEEE, IEEE, 2010*, pp. 3289–3292.
- [9] V. Bostanov, BCI competition 2003-data sets Ib and IIb: feature extraction from event-related brain potentials with the continuous wavelet transform and the t-value scalogram, *IEEE Transactions on Biomedical Engineering* 51 (6) (2004) 1057–1061.
- [10] M. Kaper, P. Meinicke, U. Grossekhoefer, T. Lingner, H. Ritter, BCI competition 2003-data set IIb: Support Vector Machines for the P300 speller paradigm, *IEEE Transactions on Biomedical Engineering* 51 (6) (2004) 1073–1076.
- [11] L. Čechovič, M. Hodoň, M. Jurečka, P300 evoked potentials data classification using feed forward neural network, *European International Journal of Science and Technology* 2 (2) (2013) 5.
- [12] E. Abdulhay, R. Oweis, A. Mohammad, L. Ahmad, Investigation of a wavelet-based neural network learning algorithm applied to P300 based Brain-Computer Interface, *Biomedical Research* (2017) S320–S324.
- [13] H. Woehrle, M. M. Krell, S. Straube, S. K. Kim, E. A. Kirchner, F. Kirchner, An adaptive spatial filter for user-independent single trial detection of Event-Related Potentials, *IEEE Transactions on Biomedical Engineering* 62 (7) (2015) 1696–1705.
- [14] T. Zeyl, E. Yin, M. Keightley, T. Chau, Partially supervised P300 speller adaptation for eventual stimulus timing optimization: target confidence is superior to error-related potential score as an uncertain label, *Journal of Neural Engineering* 13 (2) (2016) 026008.

- [15] L. Mayaud, S. Cabanilles, A. V. Langenhove, M. Congedo, A. Barachant, S. Pouplin, S. Filipe, L. Péténief, O. Rochecouste, E. Azabou, C. Hugeron, M. Lejaille, D. Orlikowski, D. Annane, Brain-computer interface for the communication of acute patients: a feasibility study and a randomized controlled trial comparing performance with healthy participants and a traditional assistive device, *Brain-Computer Interfaces* 3 (4) (2016) 197–215.
- [16] R. T. Schirrmeister, J. T. Springenberg, L. D. J. Fiederer, M. Glasstetter, K. Eggensperger, M. Tangermann, F. Hutter, W. Burgard, T. n. Ball, Deep learning with convolutional neural networks for EEG decoding and visualization, *Human Brain Mapping* 38 (11) (2017) 5391–5420.
- [17] M. Liu, W. Wu, Z. Gu, Z. Yu, F. Qi, Y. Li, Deep learning based on Batch Normalization for P300 signal detection, *Neurocomputing* 275 (2018) 288–297.
- [18] K. He, X. Zhang, S. Ren, J. Sun, Deep residual learning for image recognition, in: *2016 IEEE Conference on Computer Vision and Pattern Recognition (CVPR)*, 2016, pp. 770–778.
- [19] O. Abdel-Hamid, A. Mohamed, H. Jiang, L. Deng, G. Penn, D. Yu, Convolutional Neural Networks for Speech Recognition, *IEEE/ACM Transactions on Audio, Speech, and Language Processing* 22 (10) (2014) 1533–1545.
- [20] F. Lotte, Signal processing approaches to minimize or suppress calibration time in oscillatory activity-based Brain-Computer Interfaces, *Proceedings of the IEEE* 103 (6) (2015) 871–890.
- [21] Y. Roy, H. Banville, I. Albuquerque, A. Gramfort, T. H. Falk, J. Faubert, Deep learning-based electroencephalography analysis: a systematic review, *Journal of Neural Engineering* 16 (5) (2019) 051001.
- [22] H. Cecotti, A. Graser, Convolutional neural networks for P300 detection with application to Brain-Computer Interfaces, *IEEE Transactions on Pattern Analysis and Machine Intelligence* 33 (3) (2011) 433–445.

- [23] R. Manor, A. B. Geva, Convolutional neural network for multi-category rapid serial visual presentation BCI, *Frontiers in Computational Neuroscience* 9 (146).
- [24] S. Ioffe, C. Szegedy, Batch normalization: Accelerating deep network training by reducing internal covariate shift, in: *International Conference on Machine Learning*, 2015, pp. 448–456.
- [25] N. Srivastava, G. Hinton, A. Krizhevsky, I. Sutskever, R. Salakhutdinov, Dropout: A simple way to prevent neural networks from overfitting, *Journal of Machine Learning Research* 15 (2014) 1929–1958.
- [26] H. Shan, Y. Liu, T. Stefanov, A simple Convolutional Neural Network for accurate P300 detection and character spelling in Brain Computer Interface, in: *Proceedings of the Twenty-Seventh International Joint Conference on Artificial Intelligence, IJCAI-18, International Joint Conferences on Artificial Intelligence Organization*, 2018, pp. 1604–1610.
- [27] C. Ledesma-Ramirez, E. Bojorges-Valdez, O. Yáñez-Suarez, C. Saavedra, L. Bougrain, G. G. Gentiletti, An open-access P300 speller database, *Fourth International Brain-Computer Interface Meeting*, poster (May 2010).
- [28] M. Alvarado-González, E. Garduño, E. Bribiesca, O. Yáñez-Suárez, V. Medina-Bañuelos, P300 detection based on EEG shape features, *Computational and mathematical methods in medicine* 2016 (2016) 14.
- [29] B. Blankertz, K.-R. Muller, G. Curio, T. M. Vaughan, G. Schalk, J. R. Wolpaw, A. Schlogl, C. Neuper, G. Pfurtscheller, T. Hinterberger, et al., The BCI competition 2003: progress and perspectives in detection and discrimination of EEG single trials, *IEEE Transactions on Biomedical Engineering* 51 (6) (2004) 1044–1051.
- [30] B. Blankertz, K.-R. Muller, D. J. Krusienski, G. Schalk, J. R. Wolpaw, A. Schlogl, G. Pfurtscheller, J. R. Millan, M. Schroder, N. Birbaumer, The BCI competition III: Validating alternative approaches to actual BCI problems, *IEEE transactions on neural systems and rehabilitation engineering* 14 (2) (2006) 153–159.

- [31] A. Riccio, L. Simione, F. Schettini, A. Pizzimenti, M. Inghillefri, M. Olivetti Belardinelli, D. Mattia, F. Cincotti, Attention and P300-based BCI performance in people with amyotrophic lateral sclerosis, *Frontiers in Human Neuroscience* 7 (2013) 732.
- [32] B. Riccio, BNCI Horizon 2020: The Future of Brain/Neural Computer Interaction: Horizon 2020, <http://bnci-horizon-2020.eu/database/data-sets> (2014).
- [33] D. P. Kingma, J. Ba, Adam: A method for stochastic optimization, in: 3rd. International Conference on Learning Representations (ICLR), San Diego, USA, 2015.
- [34] F. Chollet, et al., Keras, <https://github.com/fchollet/keras> (2015).
- [35] M. Abadi, TensorFlow: Large-scale machine learning on heterogeneous systems, <https://www.tensorflow.org/> (2015).
- [36] Y. Lecun, Generalization and network design strategies, Elsevier, 1989.
- [37] I. Goodfellow, Y. Bengio, A. Courville, Deep Learning, MIT Press, 2016.
- [38] V. Nair, G. E. Hinton, Rectified linear units improve restricted Boltzmann machines, in: Proceedings of the 27th International Conference on Machine Learning (ICML-10), 2010, pp. 807–814.
- [39] D. Clevert, T. Unterthiner, S. Hochreiter, Fast and accurate deep network learning by exponential linear units (ELUs), in: International Conference on Learning Representations (ICLR), San Juan, Puerto Rico, 2016.

Table C.1: Per-subject mean AUC obtained by the architectures under analysis for within-subject P300 detection on dataset D_1 .

Subject	CNN1	UCNN1	CNN3	UCNN3	CNN-R	Deep ConvNet	Shallow ConvNet	BN ³	EEGNet	OCLNN	FCNN	SepConv1D
ACS	0.9123	0.9165	0.6894	0.7288	0.8881	0.9118	0.8249	0.8981	0.8974	0.9113	0.919	0.9129
APM	0.9314	0.9347	0.7721	0.7919	0.9177	0.9398	0.899	0.926	0.9309	0.936	0.9327	0.93
ASG	0.908	0.9108	0.771	0.7795	0.9118	0.9218	0.8969	0.9087	0.9222	0.9139	0.9073	0.9149
ASR	0.7311	0.729	0.6263	0.6397	0.7147	0.7423	0.6675	0.7316	0.7421	0.7367	0.7311	0.7302
CLL	0.8479	0.8572	0.6453	0.6616	0.8126	0.8448	0.7267	0.834	0.8309	0.8441	0.8583	0.8478
DCM	0.9421	0.9458	0.8187	0.8621	0.9353	0.9503	0.9096	0.9442	0.9404	0.9467	0.943	0.9434
DLP	0.8042	0.8206	0.6171	0.6655	0.7903	0.83	0.7324	0.791	0.8224	0.8153	0.814	0.815
DMA	0.8516	0.8667	0.6755	0.709	0.8397	0.8655	0.7499	0.8474	0.8373	0.857	0.8641	0.8599
ELC	0.9077	0.9086	0.7526	0.813	0.8939	0.9164	0.8548	0.9008	0.9022	0.9064	0.9091	0.9105
FSZ	0.9035	0.9057	0.7347	0.7724	0.8896	0.9116	0.8602	0.8977	0.9065	0.9046	0.9062	0.9081
GCE	0.8674	0.8745	0.6963	0.7533	0.852	0.8742	0.8223	0.8659	0.8673	0.8757	0.8697	0.8696
ICE	0.8882	0.893	0.7108	0.7503	0.8776	0.9013	0.7757	0.8852	0.8763	0.8916	0.8931	0.8903
JCR	0.8577	0.8713	0.7078	0.7582	0.8505	0.8746	0.8038	0.8537	0.8623	0.8667	0.8672	0.8666
JLD	0.8931	0.8931	0.7383	0.8142	0.8877	0.9051	0.8582	0.891	0.8968	0.896	0.8938	0.8929
JLP	0.8773	0.8871	0.6724	0.7177	0.8745	0.899	0.8532	0.8817	0.8864	0.8821	0.8842	0.8878
JMR	0.9187	0.9244	0.7602	0.8377	0.9061	0.925	0.8797	0.9117	0.9151	0.9185	0.929	0.9211
JSC	0.8223	0.837	0.622	0.67	0.8081	0.8483	0.748	0.8233	0.8317	0.8379	0.8388	0.8361
JST	0.9675	0.9684	0.8433	0.9121	0.9635	0.9715	0.951	0.9641	0.9699	0.9681	0.9675	0.9677
LAC	0.9379	0.9485	0.8037	0.8599	0.9457	0.9524	0.9322	0.9413	0.9438	0.9497	0.9468	0.9427
LAG	0.933	0.9353	0.6993	0.8393	0.9289	0.9435	0.9158	0.9382	0.9412	0.9406	0.9323	0.9404
LGP	0.9288	0.9338	0.8228	0.8587	0.9268	0.9399	0.8939	0.9287	0.9339	0.934	0.9348	0.9354
LPS	0.863	0.8668	0.6406	0.764	0.8473	0.871	0.802	0.8617	0.8675	0.867	0.8666	0.8636

Table C.2: Per-subject mean AUC obtained by the architectures under analysis for cross-subject P300 detection on dataset D_1 .

Subject	CNN1	UCNN1	CNN3	UCNN3	CNN-R	Deep ConvNet	Shallow ConvNet	BN ³	EEGNet	OCNN	FCNN	SepConv1D
ACS	0.8527	0.8653	0.8392	0.8366	0.8545	0.8695	0.8151	0.8725	0.8685	0.8539	0.8554	0.8727
APM	0.8453	0.8615	0.3495	0.8442	0.8468	0.8569	0.8508	0.8652	0.8706	0.8552	0.8515	0.8627
ASG	0.8680	0.8914	0.8680	0.8878	0.8892	0.8995	0.8753	0.8813	0.8972	0.8741	0.8712	0.8917
ASR	0.7260	0.7240	0.7167	0.7146	0.7293	0.7237	0.7253	0.7268	0.7332	0.7244	0.7205	0.7247
CLL	0.7009	0.7159	0.7054	0.6977	0.7036	0.7222	0.7071	0.7258	0.7195	0.7046	0.7235	0.7096
DCM	0.8332	0.8960	0.8421	0.8903	0.8819	0.8901	0.8840	0.8860	0.8899	0.8900	0.8851	0.8806
DLP	0.7687	0.7998	0.7726	0.7742	0.7907	0.7856	0.7615	0.7984	0.7969	0.7709	0.7888	0.7939
DMA	0.7542	0.8119	0.7923	0.7962	0.7791	0.7963	0.7686	0.8090	0.7994	0.7741	0.7863	0.7998
ELC	0.8433	0.8738	0.8477	0.8613	0.8758	0.8600	0.8608	0.8818	0.8747	0.8809	0.8774	0.8798
FSZ	0.8204	0.8563	0.8315	0.8496	0.8392	0.8506	0.8480	0.8625	0.8590	0.8448	0.8488	0.8579
GCE	0.8018	0.8312	0.7782	0.7932	0.8206	0.8389	0.8435	0.8317	0.8379	0.8213	0.8074	0.8193
ICE	0.7664	0.7880	0.7577	0.7660	0.7816	0.7808	0.7538	0.7810	0.7907	0.7966	0.7956	0.8044
JCR	0.8350	0.8308	0.4988	0.8241	0.8458	0.8174	0.8117	0.8390	0.8213	0.8296	0.8266	0.8274
JLD	0.8650	0.8666	0.8326	0.8415	0.8664	0.8749	0.8568	0.8656	0.8715	0.8599	0.8491	0.8632
JLP	0.8079	0.8181	0.8014	0.8061	0.8333	0.8024	0.8081	0.8197	0.8065	0.8191	0.7907	0.8070
JMR	0.8007	0.8523	0.8374	0.8378	0.8192	0.8479	0.8427	0.8337	0.8419	0.8451	0.8277	0.8406
JSC	0.7306	0.7360	0.7221	0.7119	0.7511	0.7437	0.6995	0.7291	0.7286	0.7265	0.7338	0.7326
JST	0.9125	0.9194	0.9082	0.9154	0.9105	0.9148	0.9127	0.9052	0.9251	0.9115	0.9101	0.9111
LAC	0.8395	0.9240	0.7672	0.8940	0.9211	0.9240	0.9194	0.9178	0.9245	0.9025	0.9169	0.9161
LAG	0.8217	0.8722	0.8571	0.8737	0.8666	0.8623	0.9093	0.8737	0.8960	0.8841	0.8606	0.8775
LGP	0.8704	0.8951	0.8752	0.8937	0.8930	0.9022	0.8765	0.8994	0.8966	0.8952	0.8913	0.9006
LPS	0.7923	0.8339	0.8141	0.8157	0.8030	0.8080	0.8152	0.8199	0.8257	0.8325	0.8048	0.8204

Table C.3: Per-subject mean AUC obtained by the architectures under analysis for within-subject P300 detection on datasets D_2 and D_3 .

(a) Dataset D_2												
Subject	CNN1	UCNN1	CNN3	UCNN3	CNN-R	Deep ConvNet	Shallow ConvNet	BN ³	EEGNet	OCLNN	FCNN	SepConv1D
Subject1	0.9162	0.897	0.7952	0.8458	0.9025	0.9374	0.8871	0.8522	0.9306	0.8995	0.8285	0.8933
Subject2	0.847	0.842	0.7394	0.769	0.8058	0.869	0.7477	0.7661	0.8609	0.7970	0.7372	0.8116

(b) Dataset D_3												
Subject	CNN1	UCNN1	CNN3	UCNN3	CNN-R	Deep ConvNet	Shallow ConvNet	BN ³	EEGNet	OCLNN	FCNN	SepConv1D
Subject1	0.7827	0.7657	0.6378	0.7137	0.6974	0.7980	0.7318	0.7532	0.7898	0.7527	0.7197	0.7725
Subject2	0.8590	0.8509	0.6875	0.7153	0.8123	0.8852	0.8308	0.8444	0.8727	0.8436	0.7890	0.8589

Table C.4: Per-subject mean AUC obtained by the architectures under analysis on dataset D_4

(a) Within-subject P300 detection											
Subject	CNN1	UCNN1	CNN3	UCNN3	CNN-R	Deep ConvNet	Shallow ConvNet	BN ³	EEGNet	OCLNN	SepConv1D
s0	0.8166	0.8014	0.5950	0.6358	0.8194	0.8487	0.8102	0.7850	0.8577	0.8066	0.8266
s1	0.8092	0.8040	0.6207	0.6477	0.8138	0.8475	0.8163	0.7830	0.8586	0.8048	0.8233
s2	0.8829	0.8723	0.6984	0.7559	0.8765	0.9005	0.8734	0.8742	0.8953	0.8772	0.888
s3	0.8062	0.7954	0.6666	0.6731	0.7987	0.8337	0.8059	0.8051	0.8332	0.8020	0.8093
s4	0.8514	0.8464	0.6364	0.6755	0.8583	0.8821	0.8541	0.8373	0.8800	0.8616	0.8611
s5	0.8759	0.8736	0.6449	0.7074	0.8636	0.8917	0.8644	0.8572	0.8940	0.8730	0.8798
s6	0.8538	0.8520	0.6471	0.6974	0.8715	0.8897	0.8805	0.8408	0.9067	0.8645	0.8666
s7	0.9416	0.9407	0.8416	0.8723	0.9162	0.9549	0.9454	0.9374	0.9554	0.9440	0.9457

(b) Cross-subject P300 detection											
Subject	CNN1	UCNN1	CNN3	UCNN3	CNN-R	Deep ConvNet	Shallow ConvNet	BN ³	EEGNet	OCLNN	SepConv1D
s0	0.7585	0.7361	0.7502	0.7619	0.7301	0.7370	0.7554	0.7492	0.7565	0.7546	0.7360
s1	0.7692	0.7359	0.7012	0.7126	0.7646	0.7742	0.7618	0.7467	0.7543	0.7427	0.7600
s2	0.8220	0.8344	0.8200	0.8376	0.8570	0.8275	0.8198	0.8272	0.8381	0.8369	0.8257
s3	0.7480	0.7360	0.6987	0.7471	0.7518	0.7703	0.7643	0.7585	0.7612	0.7566	0.7515
s4	0.7888	0.7687	0.7988	0.8040	0.8246	0.7970	0.8090	0.7502	0.8043	0.7529	0.7988
s5	0.8039	0.8159	0.8221	0.8269	0.7529	0.8054	0.7917	0.8028	0.8109	0.8023	0.8023
s6	0.7919	0.7724	0.7339	0.7299	0.8039	0.8210	0.7693	0.8069	0.8099	0.8001	0.7601
s7	0.8809	0.8446	0.8414	0.8411	0.8337	0.8763	0.8352	0.8491	0.8450	0.8416	0.8158

Table C.5: Number of parameters (Param) and Floating Point Operations per Second (FLOPS) of the architectures under analysis for the four benchmark datasets.

(a) D_1									
Measure	CNN1/UCNN1	CNN3/UCNN3	CNN-R	Deep ConvNet	Shallow ConvNet	BN ³	EEGNet	OCLNN	SepConv1D
Param	1,036,922	1,031,009	19,848,098	140,627	12,162	44,633	1,474	1,842	225
FLOPS	2,073,642	2,061,816	39,683,214	278,976	24,088	89,304	2,801	3,653	443

(b) D_2									
Measure	CNN1/UCNN1	CNN3/UCNN3	CNN-R	Deep ConvNet	Shallow ConvNet	BN ³	EEGNet	OCLNN	SepConv1D
Param	787,502	781,067	16,445,794	175,677	104,402	39,649	2,338	14,706	1,361
FLOPS	1,574,802	1,561,932	32,878,606	349,076	208,568	79,394	4,529	29,381	2,715

(c) D_3									
Measure	CNN1/UCNN1	CNN3/UCNN3	CNN-R	Deep ConvNet	Shallow ConvNet	BN ³	EEGNet	OCLNN	SepConv1D
Param	1,207,502	1,201,067	21,950,818	177,677	105,362	47,841	2,434	14,898	1,405
FLOPS	2,414,802	2,401,932	43,888,654	29,765	210,488	95,778	4,721	353,076	2,803

(d) D_4									
Measure	CNN1/UCNN1	CNN3/UCNN3	CNN-R	Deep ConvNet	Shallow ConvNet	BN ³	EEGNet	OCLNN	SepConv1D
Param	1,036,942	1,031,011	19,848,290	141,877	15,362	44,673	1,506	2,290	265
FLOPS	2,073,682	2,061,820	39,683,598	281,476	30,488	89,386	2,865	4,549	523